

(This is a sample cover image for this issue. The actual cover is not yet available at this time.)

This article appeared in a journal published by Elsevier. The attached copy is furnished to the author for internal non-commercial research and education use, including for instruction at the authors institution and sharing with colleagues.

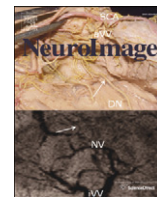
Other uses, including reproduction and distribution, or selling or licensing copies, or posting to personal, institutional or third party websites are prohibited.

In most cases authors are permitted to post their version of the article (e.g. in Word or Tex form) to their personal website or institutional repository. Authors requiring further information regarding Elsevier's archiving and manuscript policies are encouraged to visit:

<http://www.elsevier.com/copyright>

Contents lists available at [SciVerse ScienceDirect](http://SciVerse.Sciencedirect.com)

NeuroImage

journal homepage: www.elsevier.com/locate/ynimg

Spatiotemporal characteristics and vascular sources of neural-specific and -nonspecific fMRI signals at submillimeter columnar resolution

Chan Hong Moon ^{a,1}, Mitsuhiro Fukuda ^{b,1}, Seong-Gi Kim ^{b,*}

^a Department of Radiology, University of Pittsburgh, 3362 Fifth Ave, Pittsburgh, PA 15213, USA

^b Neuroimaging Laboratory, Department of Radiology, University of Pittsburgh, 3025 East Carson Street, Pittsburgh, PA 15203, USA

ARTICLE INFO

Article history:

Accepted 21 August 2012

Available online 30 August 2012

Keywords:

BOLD

CBV

Hemodynamic regulation

Orientation column

High-resolution fMRI

High fields

ABSTRACT

The neural specificity of hemodynamic-based functional magnetic resonance imaging (fMRI) signals is dependent on both the vascular regulation and the sensitivity of the applied fMRI technique to different types and sizes of blood vessels. In order to examine the specificity of MRI-detectable hemodynamic responses, submillimeter blood oxygenation level-dependent (BOLD) and cerebral blood volume (CBV) fMRI studies were performed in a well-established cat orientation column model at 9.4 T. Neural-nonspecific and -specific signals were separated by comparing the fMRI responses of orthogonal orientation stimuli. The BOLD response was dominantly neural-nonspecific, mostly originating from pial and intracortical emerging veins, and thus was highly correlated with baseline blood volume. Uneven baseline CBV may displace or distort small functional domains in high-resolution BOLD maps. The CBV response in the parenchyma exhibited dual spatiotemporal characteristics, a fast and early neural-nonspecific response (with 4.3-s time constant) and a slightly slower and delayed neural-specific response (with 9.4-s time constant). The nonspecific CBV signal originates from early-responding arteries and arterioles, while the specific CBV response, which is not correlated with baseline blood volume, arises from late-responding microvessels including small pre-capillary arterioles and capillaries. Our data indicate that although the neural specificity of CBV fMRI signals is dependent on stimulation duration, high-resolution functional maps can be obtained from steady-state CBV studies.

© 2012 Elsevier Inc. All rights reserved.

Introduction

The neural specificity of the hemodynamic-based functional magnetic resonance imaging (fMRI) signal is mainly determined by two factors, i.e., the vascular regulation and the sensitivity of the functional imaging technique to microvessels, including arterioles, capillaries, and venules. In order to examine the spatial neural specificity of fMRI signals, it is necessary to use small biological functional units intrinsically represented in the brain, while excluding any vascular implication. For this purpose, the cortical functional columns representing somatotopy (e.g., whisker barrels), ocular dominance and orientation preference (Hubel and Wiesel, 1963; Mountcastle, 1957; Woolsey and Van der Loos, 1970) can be used. Particularly, the orientation column is preferable over somatotopy and ocular dominance column due to the following reasons. First, the whisker barrel fields and ocular dominance columns are both functionally

and anatomically defined, and may have a one-to-one relationship with the corresponding vascular territories, as found in the whisker barrel field (Cox et al., 1993) and the ocular dominance column (Shmuel et al., 2010). However, the orientation column is not anatomically definable and its vascular regulation is not determined by anatomical segregation. Second, iso-orientation columns extend throughout the entire cortical plate and repeat about every millimeter, so multiple sampling points can be collected in fMRI. Orthogonally oriented stimuli (e.g., horizontal vs. vertical grating bars) induce neural activity in complementary columnar domains; spiking activity evoked for an orientation stimulus is localized only to columns preferring the orientation stimulus, and is minimal within columns preferring the orthogonal stimulus (Grinvald et al., 1986; Hubel and Wiesel, 1962). Thus, column-specific and -nonspecific hemodynamic responses can be separated by subtracting the responses of orthogonal stimuli from one another (e.g., Fukuda et al., 2005), and the active column-specific signals can be considered to be neuronally specific. Functional columns have been successfully mapped largely in primary visual cortex by high-resolution fMRI (Chen et al., 2007; Cheng et al., 2001; Dechent and Frahm, 2000; Duong et al., 2001; Fukuda et al., 2006a; Kim et al., 2000; Menon et al., 1997; Moon et al., 2007; Yacoub et al., 2008; Zhao et al., 2005), indicating that neural-specific signals exist in submillimeter high-resolution fMRI. However, the

* Corresponding author at: Departments of Radiology and Neurobiology, University of Pittsburgh, 3025 East Carson Street, Pittsburgh, PA 15203, USA. Fax: +1 412 383 6799.

E-mail addresses: moonc@upmc.edu (C.H. Moon), mif5@pitt.edu (M. Fukuda), kimsg@pitt.edu (S.-G. Kim).

¹ CHM and MF contributed equally to this work.

spatiotemporal characteristics of neural-specific and -nonspecific submillimeter fMRI signals and their relationship with the cortical vasculature remain poorly understood.

The degree of neural-specificity of fMRI signals can be changed with different hemodynamic signal sources, e.g., blood oxygenation level-dependent (BOLD) vs. cerebral blood volume (CBV), and different response times, e.g., early vs. late response (e.g., 3–5 s vs. 18–20 s). The major difference between BOLD and CBV responses is the contribution of blood draining effects. In BOLD studies, spatial specificity is progressively lost after stimulus onset, largely due to venous draining in an anterograde manner following stimulation (Fukuda et al., 2006b; Nagaoka et al., 2005). In CBV studies, time-dependent spatial specificity is closely dependent on vascular regulation mechanisms. If vasoactive signals from highly-localized capillaries dilate larger arterial vessels in a retrograde manner, then the earlier CBV response should be more specific than the later response. This appears to be supported by an optical imaging study in the whisker barrel cortex (Sheth et al., 2005). However, in layer-dependent CBV studies (Jin and Kim, 2008; Kim and Kim, 2010), the later response is more specific to layer IV than the early response (> 12 s vs. 3–5 s after stimulus onset in Fig. 3, Jin and Kim, 2008), suggesting that the late CBV response could be more specific to neural activity. These conflicting findings of CBV specificity can be due to different vasculatures in cortical columns and layers, and different vessel sensitivities of optical imaging and fMRI to pial vs. parenchymal vessels. Key questions remain whether the intracortical vasculature is organized to represent columnar structure and how the vasculature is regulated by local neural activity.

In the present study, the spatiotemporal characteristics of neural-specific and -nonspecific fMRI responses and their relationship to intracortical vascular structure were investigated in a well-established cat orientation column model. Orientation columns in cat visual cortex are extensively-investigated functional structures by electrophysiology (Hubel and Wiesel, 1962; Hubel and Wiesel, 1963), intrinsic optical imaging (Bonhoeffer and Grinvald, 1993; Das and Gilbert, 1995; Fukuda et al., 2005, 2006b; Grinvald et al., 1986; Malonek and Grinvald, 1996; Vanzetta et al., 2004a) and fMRI (Duong et al., 2001; Fukuda et al., 2006a; Kim et al., 2000; Moon et al., 2007; Tanaka et al., 2011; Zhao et al., 2005). High-resolution BOLD and CBV fMRI data were acquired at 9.4 T before and after injection of a contrast agent, respectively. Intracortical venous vasculature was obtained from high-resolution venographic MR anatomy image, and baseline blood volume map was acquired with the aid of a contrast agent. Spatiotemporal characteristics of BOLD and CBV responses were examined in the cortical surface to the parenchyma. Orientation-specific and -nonspecific BOLD and CBV activations were analyzed by comparing with venographic image and baseline blood volume map on a pixel-by-pixel basis.

Methods and materials

Animal preparation

Ten cats (1.3–2.5 kg) were used with approval by the Institutional Animal Care and Use Committee at the University of Pittsburgh following the National Institutes of Health guidelines; five were used for low-resolution fMRI (i.e., 312- μm resolution) and another five for high-resolution fMRI (i.e., 156- μm). After treatment with atropine sulfate (0.05 mg kg⁻¹, intramuscular injection (IM)), each cat was initially anesthetized with a cocktail of ketamine (10–20 mg kg⁻¹, IM) and xylazine (1 mg kg⁻¹, IM), and ventilated with 2% isoflurane in oxygen-enriched air (30–35% inspired O₂) during catheterization. After catheterizing the femoral artery for blood pressure monitoring and the femoral vein for supplemental liquid infusion, the cat was placed in a cradle and secured in a postural position with a custom-designed head frame in the magnet. Each cat

was fitted with appropriate contact lenses and was paralyzed with pancuronium bromide (0.2 mg kg⁻¹ h⁻¹). Isoflurane level was decreased to 1.0–1.2% for the functional tasks. Rectal temperature, mean arterial blood pressure and end-tidal CO₂ gas were maintained at 38.0 ± 0.2 °C, 90–100 mmHg and 3.4–3.6%, respectively.

Visual stimulation

Visual responses were induced by binocularly presenting moving, full-field, square-wave, black-white gratings of different orientations (100% contrast, 0.15 cycle/° of visual field, 2 cycles s⁻¹, moving direction reversal per 0.5 s). In each animal, conventional block-design and continuous stimulation paradigms were used.

- 1) To investigate the characteristics of orientation-specific and -nonspecific signals, block-design experiments were performed.
 - (i) In low-resolution studies (see later for details of MRI parameters), we presented a 20-s long orientation stimulus (67.5°) flanked by a 20-s pre-stimulus and a 20-s post-stimulus baseline period, in which a homogeneous gray background was presented with the same average luminance as black–white grating stimuli.
 - (ii) In high-resolution studies (see later), four orientations (0°, 45°, 90° and 135°, 10-s each) were interleaved with a 10-s homogeneous gray background. The 80-s cycle was repeated 11 times to increase our signal-to-noise ratio.
- 2) To determine the iso-orientation columnar maps and define regions of interest for the analyses of aforementioned two different block-design data, we used continuous stimulation consisting of eight consecutive orientations (0° to 157.5° with 22.5° step, 10-s each; total 80-s stimulation) without any inter-stimulus interval and repeated 11 times. This paradigm has proven effective in obtaining iso-orientation maps (Fukuda et al., 2006a; Moon et al., 2007).

MRI experiments

All MRI was performed on a 9.4-T/31-cm horizontal MR system (Varian Inc., Palo Alto, CA) with an active shielded gradient coil operating at a maximum strength of 400 mT/m and a rise time of 120 μs . A custom-made surface radio frequency (RF) coil (16-mm diameter) was positioned over the visual cortex. A three-dimensional (3-D) venographic image was obtained to determine the functional imaging slice using flow-compensated RF-spoiled gradient-echo (GE) sequence (Park et al., 2008) with data matrix = 512 × 256 × 256, field of view (FOV) = 35 × 22 × 22 mm³, resolution = 68 × 86 × 86 μm^3 , repetition time (TR) = 50 ms, and echo time (TE) = 20 ms. For functional studies, a single slice of 1-mm thickness was selected either along the axial orientation below the surface in the parenchyma (Fig. 1A) or the sagittal orientation along the medial bank of the visual cortex (white rectangle in Fig. 2A). Once a slice position was determined, a 1-mm thick T₂*-weighted venographic image was acquired using two-dimensional GE sequence with data matrix = 256 × 256, FOV = 20 × 20 mm², TR = 50 ms, and TE = 15–20 ms as an anatomical reference.

In low-resolution studies (n = 5 cats), fMRI data in the axial plane were obtained using a gradient echo planar imaging (EPI) technique with data matrix = 64 × 64, FOV = 20 × 20 mm², pixel resolution = 312 × 312 μm^2 and TR = 0.5–1.0 s. In high-resolution fMRI studies (n = 5 cats), data in the sagittal plane were obtained using a four-segmented, center-out EPI technique with data matrix = 128 × 128, FOV = 20 × 20 mm², pixel resolution = 156 × 156 μm^2 and TR = 2 s. Navigator echo was acquired at each echo-train segment before the application of phase-encoding and readout gradient for the correction of inter-segment phase and magnitude modulations due to a respiration or unknown physiology changes (Kim et al., 1996). In

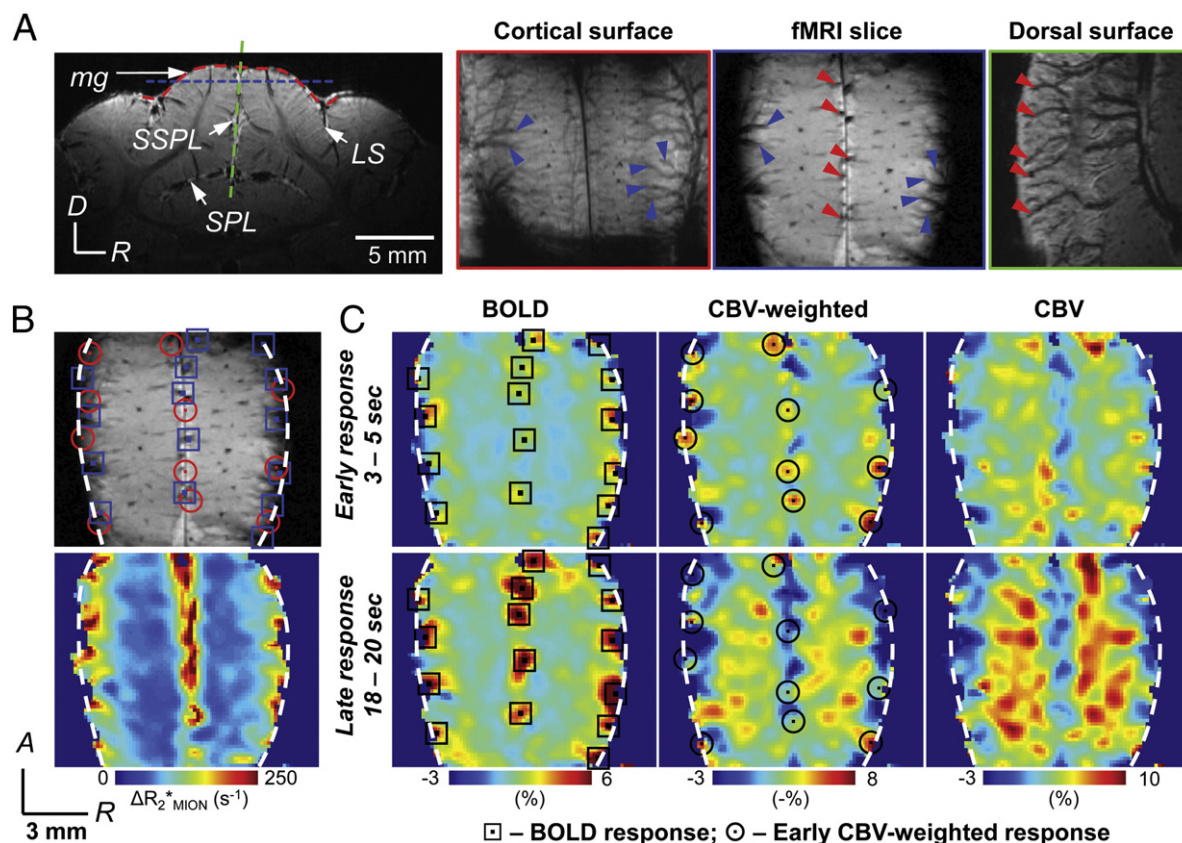


Fig. 1. Pial vs. parenchymal activations in low-resolution fMRI. A, Vasculature on the cortical surface. (Left most) T_2^* -weighted anatomical image in coronal view. Curve and straight dotted lines are the positions of reconstructed images shown in 2nd to 4th panel; the red curve follows the cortical surface of marginal gyrus (corresponding to 2nd panel image), the horizontal blue line is the position of the functional imaging slice (corresponding to 3rd panel image), and the almost-vertical green line is the position of the midline sagittal image (corresponding to 4th panel). Large pial vessels running across the cortical surface (blue arrowheads in 2nd panel) or midline (red arrowheads in 4th panel) were identified, and marked on the fMRI slice (3rd panel). B, T_2^* -weighted anatomical image (top) and the baseline blood volume map (bottom) of the functional imaging slice. Hypointense pixels in the T_2^* -weighted image have large baseline blood volume (red pixels in ΔR_{2MION}^*). White-dashed lines represent the surface boundary of the cortex. C, Single-condition maps of BOLD, CBV-weighted, and relative CBV at 3–5 s (top panels) and 18–20 s (bottom panels) after stimulus onset. Black/red circles (\odot) and black/blue rectangles (\square) are the foci in CBV-weighted maps at early response time and BOLD activation maps, respectively, and are overlaid on images A and B. Note that the hot foci of CBV-weighted and BOLD maps do not coincide with each other. Patchy functional structures were observed within the cortex at early and late relative CBV maps. Abbreviations: LS, lateral sulcus; SPL, suprasplenial sulcus; SSPL, secondary suprasplenial sulcus; mg, marginal gyrus; D, dorsal; R, right; A, anterior. Same abbreviations are used in the following figures. (For interpretation of the references to color in this figure legend, the reader is referred to the web version of this article.)

each subject, block-design and continuous stimulation fMRI studies were performed.

- 1) Block-design studies: BOLD with TE = 18 ms and CBV-weighted fMRI with TE = 10 ms were acquired before and after the intravenous bolus injection of a monocrystalline iron oxide nanoparticle (MION) contrast agent into the femoral vein. MION has a long intravascular half-life and distributes throughout the blood plasma in the cortical vessels; fMRI signals with iron oxide are mainly weighted by changes in plasma CBV (Mandeville et al., 1998; Zhao et al., 2006). In addition, EPI images (without any stimulation) with TE = 10 ms were acquired before and after the MION administration to quantify baseline CBV, ΔR_{2MION}^* .
- 2) Continuous stimulation study: CBV-weighted fMRI with TE = 10 ms was obtained.

Data analysis

All data were analyzed with home-made programs coded using either Visual C++ (Microsoft, CA) or Matlab (The MathWorks, MA). Low- and high-resolution functional MR images were zero-padded to 128×128 and 256×256 matrix, respectively. A low-pass Hanning filter was applied in K -space to remove high-frequency noise and ringing artifacts caused by zero-padding. All fMRI runs

for each experiment were averaged; three averaged fMRI data sets (i.e., block-design stimulation BOLD and CBV-weighted, and continuous stimulation CBV-weighted data) were produced. The first 80-s data for continuous and 4-orientation block-design stimulation was disregarded in the processing to consider only steady-state functional condition.

In each animal, baseline ΔR_{2MION}^* was determined as $\ln(S_{pre}/S_{post})/TE$ where S_{pre} and S_{post} are the EPI intensity signals before and after MION injection, respectively (Zhao et al., 2006). Pixel-wise ΔR_{2MION}^* value indicates the relative baseline CBV distribution, and was used to convert from a CBV-weighted fMRI signal to a quantitative relative CBV change (simply termed as ‘CBV’ afterward).

Generation of iso-orientation map from continuous stimulation data

In order to calculate an iso-orientation map from CBV-weighted fMRI data with continuous stimulation, the response in each pixel was modeled using a sinusoidal function, with magnitude and phase, at a specific stimulation frequency, f_s , as follows:

$$\Delta S(x, y, t) = M(x, y) \cos\{2 \cdot \pi \cdot f_s \cdot t + \Phi(x, y)\} \quad (1)$$

where $\Delta S(x, y, t)$ is the signal at position x and y at time t , $M(x, y)$ and $\Phi(x, y)$ are the magnitude and phase map at f_s . The magnitude and phase maps at f_s can be calculated by Fourier analysis (Fukuda et

al., 2006a; Kalatsky and Stryker, 2003; Moon et al., 2007). Continuous stimulation data were initially divided by the mean baseline DC signal; thus $M(x,y)$ is the magnitude percentage change and $\Delta S(x,y,t)$ is the percentage signal change with phase information (i.e., iso-orientation map at a given time, t). The hemodynamic delay must be corrected in the phase map, which is ~ 13 s for CBV fMRI orientation-specific response (Fukuda et al., 2006a; Moon et al., 2007). Thus, the iso-orientation map, $\Delta S(x,y)$ corresponding to 0° stimulation (presented for 0–10 s) was obtained at $t = 13$ s with $f_s = 1/80 \text{ s}^{-1}$ (i.e., 0.0125 Hz) in Eq. (1); 45° at $t = 33$ s (i.e., $13 \text{ s} + 80 \text{ s} \times (45^\circ/180^\circ)$); 67.5° at $t = 43$ s, etc. The CBV-weighted iso-orientation map was converted into a

relative CBV change map as $-\Delta S(x,y)/TE$ divided by baseline total blood volume, ΔR_{2MION}^* .

Generation of functional activity maps from block-design stimulation data

In each animal, BOLD and CBV-weighted maps were calculated. For low-resolution imaging studies, single-condition maps were calculated in percent change by subtracting the averaged baseline image for the pre-stimulus 10-s period from images obtained during 20-s stimulation, and then dividing the images by the averaged baseline image. Then, two averaged single-condition percent change

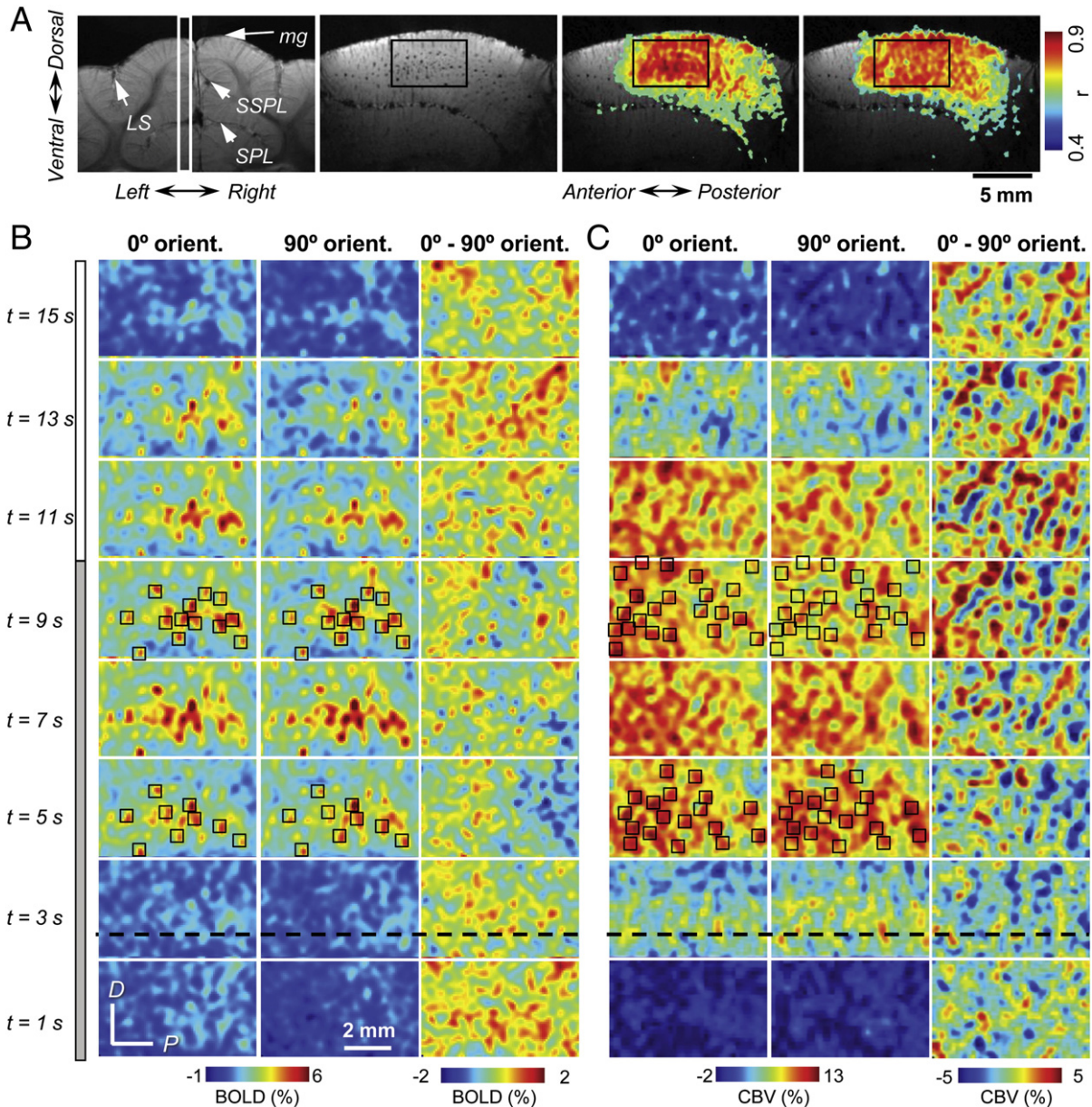


Fig. 2. Spatiotemporal changes of high-resolution BOLD and CBV maps. **A**, Imaging slice and ROI selection. (1st panel) Axial view image of cat visual cortex reconstructed from 3-D venogram. A functional imaging slice (white rectangle) is positioned perpendicular to the axial plane to cover the medial bank of the visual cortex. (2nd panel) T_2^* -weighted image at the functional imaging position. (3rd and 4th panels) BOLD and CBV-weighted cross-correlation activation maps. Analysis ROI (black rectangle) is placed on a common active area in BOLD and CBV-weighted maps. **B** and **C**, Spatiotemporal changes of BOLD and CBV activations in the analysis ROI. (1st to 3rd column panels) Single-condition 0° and 90° activation maps, and differential maps between 0° and 90° stimulus at every 2 s. To assist comparison, open squares (\square) are placed on strong activation regions in 0° single-condition maps at 5 s and 9 s, and overlaid on 90° single-condition maps. Note that while the sites of high BOLD signals to 0° stimulus coincide with those to 90° stimulus over stimulation period, the sites of high CBV signals to 0° and 90° stimulus coincide at early stimulation time, but are separated at late and even post-stimulation time points. Stimulation time from the onset is presented in the left of the figure; a gray bar for stimulation period (10 s) and white for post-stimulation period (6 s). Supplementary to this figure, Supplementary Fig. 1 is shown with the full range of color scale for each image to maximize the contrast of activation patterns.

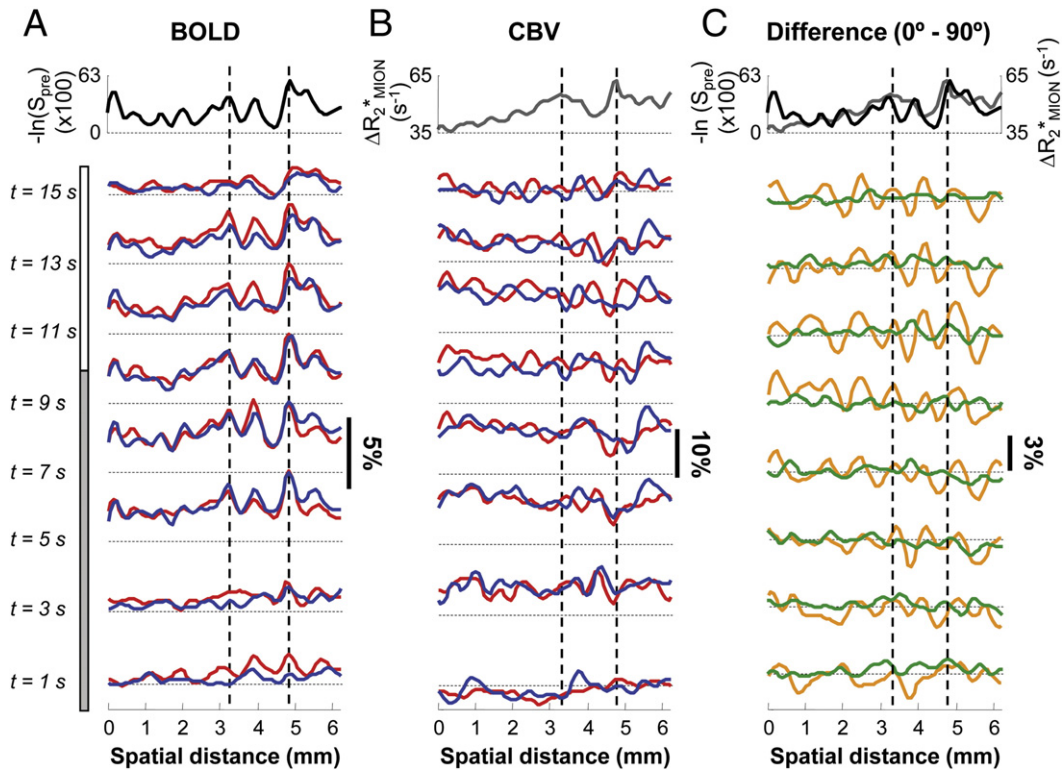


Fig. 3. Temporal changes of high-resolution BOLD and CBV activation profiles. The data were obtained along the black-dashed lines shown in Figs. 2B and C. A and B, Profiles of single-condition BOLD and CBV activations. Baseline blood volume profiles before and after MION injection (i.e., $-\ln(S_{pre})$ and ΔR_{2MION}^*) are presented in the top panels (black and gray traces). Red and blue traces represent the responses to 0° and 90° stimuli, respectively. C, Profiles of differential BOLD (green traces) and CBV activations (orange traces). A black-dotted horizontal line indicates 0% functional changes at each time point. Stimulation time from the onset is presented in the left of the figure; a gray bar for stimulation period (10 s) and white for resting (6 s). Vertical broken lines indicate a representative large vessel position. (For interpretation of the references to color in this figure legend, the reader is referred to the web version of this article.)

maps were generated; an early response map averaging between 3 and 5 s after stimulus onset, and a late response map averaging between 18 and 20 s.

For high-resolution imaging studies, four different functional activity maps were generated. i) Single-condition maps were generated in percent change with an average of 6-s pre-stimulus images as a baseline. ii) Differential maps were calculated by subtracting single-condition maps responding to orthogonal stimuli (0° – 90° , 45° – 135° , 90° – 0° , and 135° – 45°). The differential map faithfully represents the sites of orientation-selective neural activities only if the responses to orthogonal orientation simulation are subtracted (Grinvald et al., 1986; Shoham et al., 1999). iii) Orientation-nonspecific magnitude maps were obtained from $M(x,y)$ at $f_s = 1/20 \text{ s}^{-1}$ in Eq. (1). iv) Orientation-specific magnitude maps were obtained from $M(x,y)$ at $f_s = 1/80 \text{ s}^{-1}$ in Eq. (1). Note that orientation-specific BOLD signal was minimal and thus not considered in orientation-specific CBV calculation. The analysis in the frequency domain is advantageous for the periodic stimulus data compared to the time domain analysis because of more effective averaging and better suppression of slow physiological noises. Phase maps of orientation-specific CBV responses were obtained from $\Phi(x,y)$ in Eq. (1) with the compensation of the 13-s hemodynamic delay.

Since CBV-weighted fMRI contains BOLD signals, the BOLD contribution to CBV-weighted signal was removed and divided by baseline total blood volume, ΔR_{2MION}^* for obtaining quantitative relative CBV changes (Zhao et al., 2006) as

$$\text{CBV} = \left\{ -\frac{\Delta S}{\text{TE}} \Big|_{\text{CBV-weighted}} + \frac{\Delta S}{\text{TE}} \Big|_{\text{BOLD}} \right\} / \Delta R_{2MION}^* \quad (2)$$

where ΔS is the percent signal of CBV-weighted and BOLD fMRI data (see Fig. 1).

Quantitative analyses of block-design stimulation data

To determine the temporal characteristics of hemodynamic responses, iso-orientation regions of interest (ROI) were determined from continuous stimulation CBV data by thresholding the iso-orientation maps with a $[\text{Mean} + 1 \cdot \text{SD}]$, where the *Mean* and *SD* were obtained from all pixel values. Reasons to use continuous stimulation data for the ROI selections are that i) iso-orientation maps obtained from continuous data were confirmed by intrinsic optical imaging (Fukuda et al., 2006a), and ii) ROIs were independently determined from block-design stimulation data, thus minimizing bias. Two iso-orientation ROIs (67.5° vs. 157.5° , orthogonal to each other) were determined for low-resolution imaging studies; the mean area of these iso-orientation ROIs was $10.6 \pm 5.0 \text{ mm}^2$ ($n=5$ cats and 2 orientation ROIs for each cat), which corresponds to ~ 430 pixels. Four iso-orientation ROIs (0° , 45° , 90° , and 135°) were determined for high-resolution studies; the mean area of the iso-orientation ROIs was $3.0 \pm 0.7 \text{ mm}^2$ ($n=5$ cats and 4-orientation ROIs for each cat), which corresponds to ~ 490 pixels.

Then, the preferred and nonpreferred responses within the ROIs were determined from block-design stimulation data. For low-resolution data, the preferred and nonpreferred responses to 67.5° stimulus were determined from 67.5° and 157.5° iso-orientation ROIs, respectively (Note: only one stimulus orientation was used in this block-design stimulation). For high-resolution data, the preferred and nonpreferred responses within one iso-orientation ROI (e.g., 0°) were determined by the block-design response to the corresponding (e.g., 0°) and orthogonal stimulus (e.g., 90°), respectively. Similarly, the preferred and nonpreferred responses were

obtained from four iso-orientation ROIs, and averaged. Then, neural (orientation)-specific signals were obtained by subtracting the nonpreferred response from the preferred response, while the nonpreferred responses were defined as neural-nonspecific signals. To quantify the degree of fMRI localization to cortical columns, a spatial specificity index was calculated as (orientation-specific signal) / (orientation-specific + orientation-nonspecific signals). This will be close to '1' if the neural-specific signal is dominant, and close to '0' if the nonspecific signal is dominant. Temporal characteristics of the orientation-specific and -nonspecific responses were examined for 10-s (with 10-s inter-stimulus interval) high-resolution data and 20-s stimulus low-resolution block-design stimulus data.

Relationship between high-resolution fMRI signals and the vasculature

In order to characterize the vascular origin of fMRI signals in the parenchyma, only high-resolution data were used because of its superiority in visualizing intracortical vessels. All intracortical veins were identified from T_2^* -weighted venographic GE images. The anatomical image was smoothed to match the spatial resolution of EPI, and spatial intensity inhomogeneity induced by a surface RF coil was reduced by applying a high pass-filter with a bandwidth of 3 mm^{-1} (removing spatial signal variations with $>3\text{-mm}$ width). Local minima were selected as venous vessels. The baseline venous CBV index before the MION injection was calculated by $-\ln(S_{pre})$ where S_{pre} is the EPI intensity scaled to [0, 1]. Neural-specific and -nonspecific signals were compared with the vascular image, venous CBV index, $-\ln(S_{pre})$, and the baseline total CBV, ΔR_{2MION}^* .

Statistical analyses

Statistical analysis of data between BOLD and CBV was performed by analysis of variance (ANOVA). If a significant difference was found, the Student's *t*-test (paired, two-tailed) was performed. The probability (*P*) value of <0.05 was considered as statistically significant. Data are presented as *Mean* \pm *SD*.

Results

Spatiotemporal characteristics of pial BOLD and CBV responses

In order to visualize pial vessel responses during stimulation, the 1-mm thick imaging slice was selected tangential to the cortical surface (Moon et al., 2007), and the activation maps of BOLD and CBV changes at two time periods (i.e., early vs. late response time) were obtained from low-resolution fMRI data (Fig. 1). Pial vessels were identified with 3-D venographic image. Pial vessels in the fMRI slice (blue/red arrowheads in Fig. 1A 3rd panel) were traced from identifiable pial vessels in the cortical surface image (blue arrowheads in 2nd panel), and the sagittal midline image (red arrowheads in 4th panel) reconstructed from 3-D image. Total baseline blood volume, ΔR_{2MION}^* , was mostly higher in the pia than the parenchyma, mainly due to contributions of large vessels in the cortical surface (lower panel in Fig. 1B). The highest amplitude BOLD signals (black/blue rectangles) were always observed in the cortical surface regardless of the response times but with different intensities (left column panels in Fig. 1C). Most hot spots of BOLD activations were coincident with hypointense pixels, indicating pial veins. The highest CBV-weighted responses were located on the cortical surface at the early response time (see black circles in middle column panels in Fig. 1C), but in the parenchyma at the late response time. Interestingly, the hot spots in the early response CBV-weighted maps at the cortical surface (red circles in Fig. 1B) were not co-registered to those of BOLD maps (blue rectangles in Fig. 1B), indicating that pial vessels with early CBV responses might be arterial, and not of venous origin. When CBV-weighted fMRI signals (middle column panels in Fig. 1C) were divided by the baseline total blood volume, relative CBV changes were determined (right column panels in Fig. 1C). In the CBV change maps, pial vessel responses were significantly reduced relative to the parenchyma, indicating that even if absolute CBV change is higher in (large) pial vessels than (small) parenchymal vessels, its relative change can be less. Parenchymal CBV

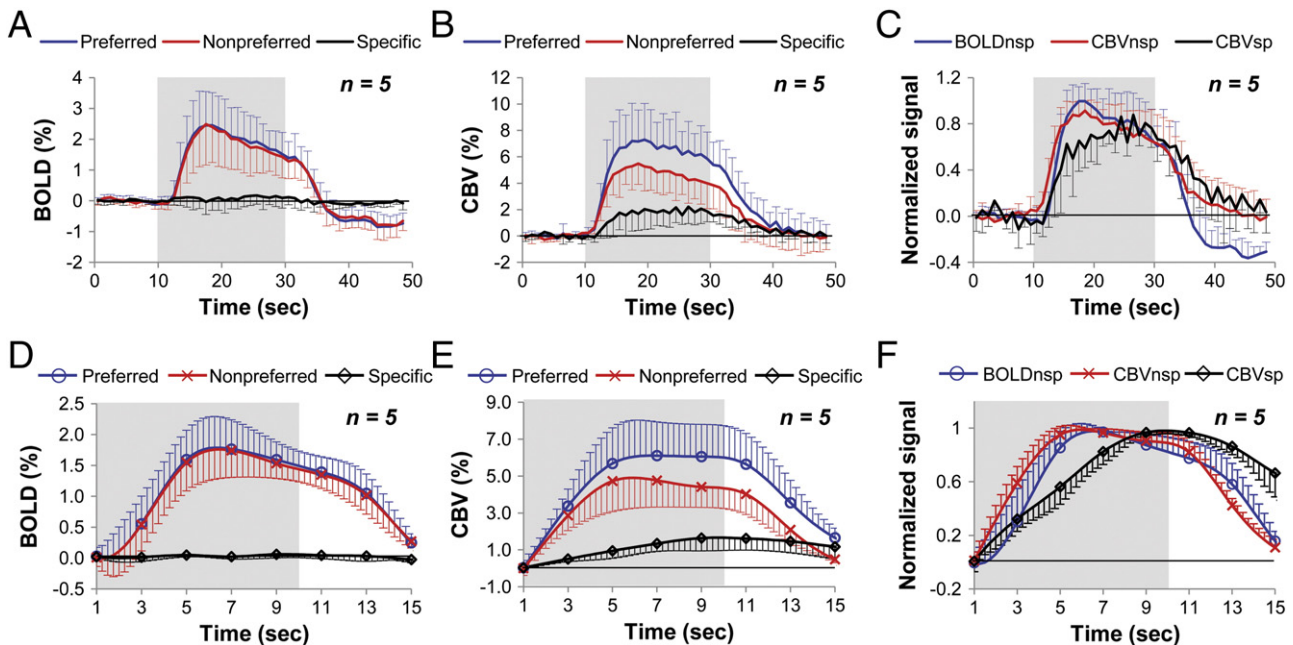


Fig. 4. Time courses of orientation-specific and -nonspecific fMRI signals. A and B, BOLD and CBV responses to 20-s long stimulation. D and E, BOLD and CBV responses to 10-s long stimulation. Specific response (black trace) is obtained by subtraction of the nonpreferred response (red trace) from the preferred response (blue trace). C and F, Temporal dynamics of the normalized nonspecific (i.e., nonpreferred) and specific responses for 20-s and 10-s long stimulation periods. Functional responses in each cat were normalized to their peak signals before averaging. Note that specific CBV response is slower than nonspecific CBV and BOLD responses and is sustained even after the cessation of stimulation. BOLD_{nsp}, CBV_{nsp} and CBV_{sp} stand for the orientation-nonspecific BOLD, -nonspecific CBV and -specific CBV signal, respectively. Experimental data in D–F were acquired every 2 s (×, ○, symbols) and interpolated with the B-spline method. Error bars are SD of mean (n = 5 cats). The gray bars indicate a stimulation period. (For interpretation of the references to color in this figure legend, the reader is referred to the web version of this article.)

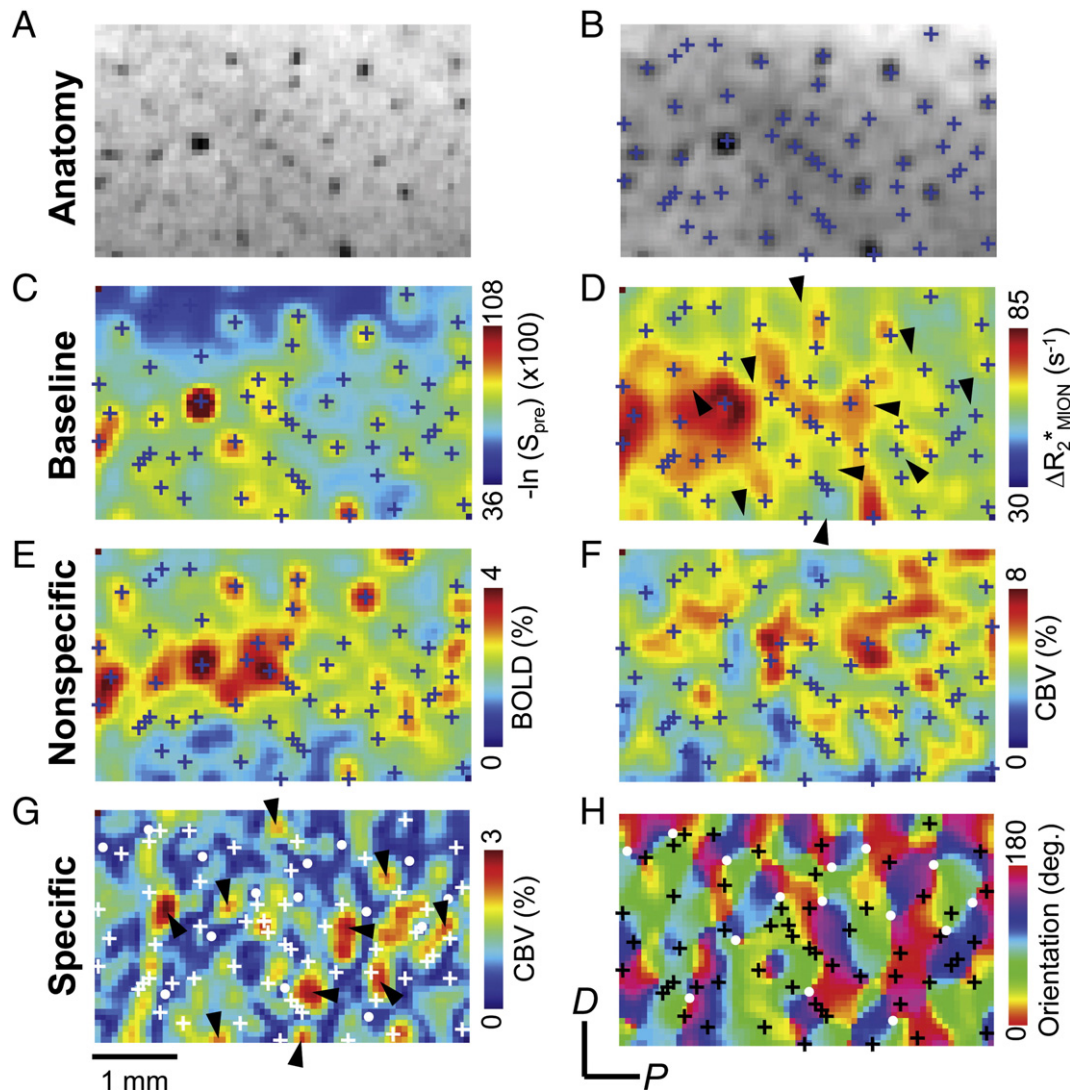


Fig. 5. Relationships between fMRI activations and vasculature. A and B, Original and filtered T_2^* -weighted GE anatomy image. Local minima of image intensity are determined from B and overlaid on C through H (blue/black/white crosses). C and D, Baseline venous blood volume index, $-\ln(S_{pre})$ and baseline total blood volume index, ΔR_{2MION}^* . Black arrowheads in panel D mark representative high orientation-specific CBV foci (see panel G). E and F, Nonspecific BOLD and CBV magnitude maps. Note that the sites of high BOLD signals coincide well with the intracortical venous vessel locations. G and H, Specific CBV magnitude and orientation composite phase maps. Representative pinwheel centers (or fractures) and high specific CBV signal foci are marked with solid white dots and black arrowheads, respectively. (For interpretation of the references to color in this figure legend, the reader is referred to the web version of this article.)

responses were not homogeneous, but patched like columns (right-lower column panel in Fig. 1C).

Spatiotemporal characteristics of parenchymal BOLD and CBV activations

To examine the spatiotemporal patterns of parenchymal BOLD and CBV changes, high-resolution fMRI data were used. To maximize the primary visual cortical area in the imaging plane, a single 1-mm thick flat slice was selected in sagittal plane along the medial bank of visual cortex (white rectangle in Fig. 2A). A rectangular region was manually chosen from a commonly activated region in BOLD and CBV-weighted fMRI maps with a cross-correlation (r) value of >0.5 as an ‘analysis’ ROI (black rectangle in Fig. 2A) for further analyses; the mean ROI area was $17.7 \pm 4.6 \text{ mm}^2$ ($n = 5$ cats). The ROI is most parallel to the cortical surface (see many dark spots in the anatomical image; the vessels perpendicular to the cortical surface appear as dark spots). Functional columnar domains are not readily visible in the single-condition maps (see 1st and 2nd columns in Figs. 2B and C) because large orientation-nonspecific signals obscure the small specific signals. To detect only the orientation-specific signals, differential

maps are created by subtracting single-condition maps of 90° stimulus from those of 0° stimulus (see 3rd columns in Figs. 2B and C). In the differential maps, dark red pixels (positive values) have higher response to the 0° stimulation, while dark blue pixels (negative values) have higher response to the 90° stimulation. To better visualize the spatiotemporal changes in BOLD and CBV responses, their spatial profiles were obtained along the black-dashed horizontal lines (shown at $t = 3$ s in Figs. 2B and C), and plotted in Fig. 3 with baseline blood volume profiles. For Fig. 3, the $-\ln(S_{pre})$ obtained from the baseline EPI before MION injection is sensitive to the venous blood volume fraction, while the ΔR_{2MION}^* (s^{-1}) induced by MION is sensitive to the total blood volume including venous volume.

BOLD responses became visible at 4 s after stimulus onset, and peaked at 7 s (Fig. 2B). Time-dependent, single-condition BOLD activation maps of 0° and 90° stimuli were apparently indistinguishable – the strong activation sites to 0° stimulation were well matched to those to 90° stimulation (see black square regions in Fig. 2B). These 0° and 90° single-condition BOLD maps were highly correlated to each other ($r = 0.66 \pm 0.14$ from 3 s to 11 s, $P < 0.001$, $n = 5$ cats). Their activation

profiles were very similar to each other (Fig. 3A), and were well correlated to the venous blood volume fraction (see dashed vertical lines). Thereby, although orientation-nonspecific responses were removed by the subtraction method, differential maps (3rd column in Fig. 2B) and profiles (green traces in Fig. 3C) did not show consistent visible columnar structures at any time point.

Single-condition CBV activation maps (Fig. 2C) and profiles (Fig. 3B) responding to either 0° or 90° stimulation looked similar at 3–5 s after stimulus onset, but became different at 9–11 s (see black square regions in Fig. 2C). Correlation coefficients between two CBV maps at 3–5 s were indeed significantly higher than those at 9–11 s; $r = 0.48 \pm 0.18$ vs. 0.27 ± 0.08 ($P < 0.05$, $n = 5$ cats). Consequently, differential CBV maps and profiles clearly and consistently showed the iso-orientation columnar patches and patterns, particularly at 9–11-s data points (3rd column in Fig. 2C and orange traces in

Fig. 3C). Distance between the peaks corresponding to 0° columns (Fig. 3C) was ~1 mm, which is consistent with the known inter-columnar distance of 1–1.4 mm (Fukuda et al., 2005; Löwel et al., 1987). Single-condition and differential CBV profiles did not show any obvious relationship with the total baseline blood volume (see dashed vertical lines in Figs. 3B and C).

Overall, our fMRI data indicate that 1) the single-condition BOLD activation has a dominant nonspecific signal component, and 2) the early CBV activation is less localized to active orientation columns, than the late CBV activation.

Temporal characteristics of parenchymal BOLD and CBV fMRI responses

To further examine the temporal dynamics of BOLD and CBV functional responses, the time-courses of block-design stimulation

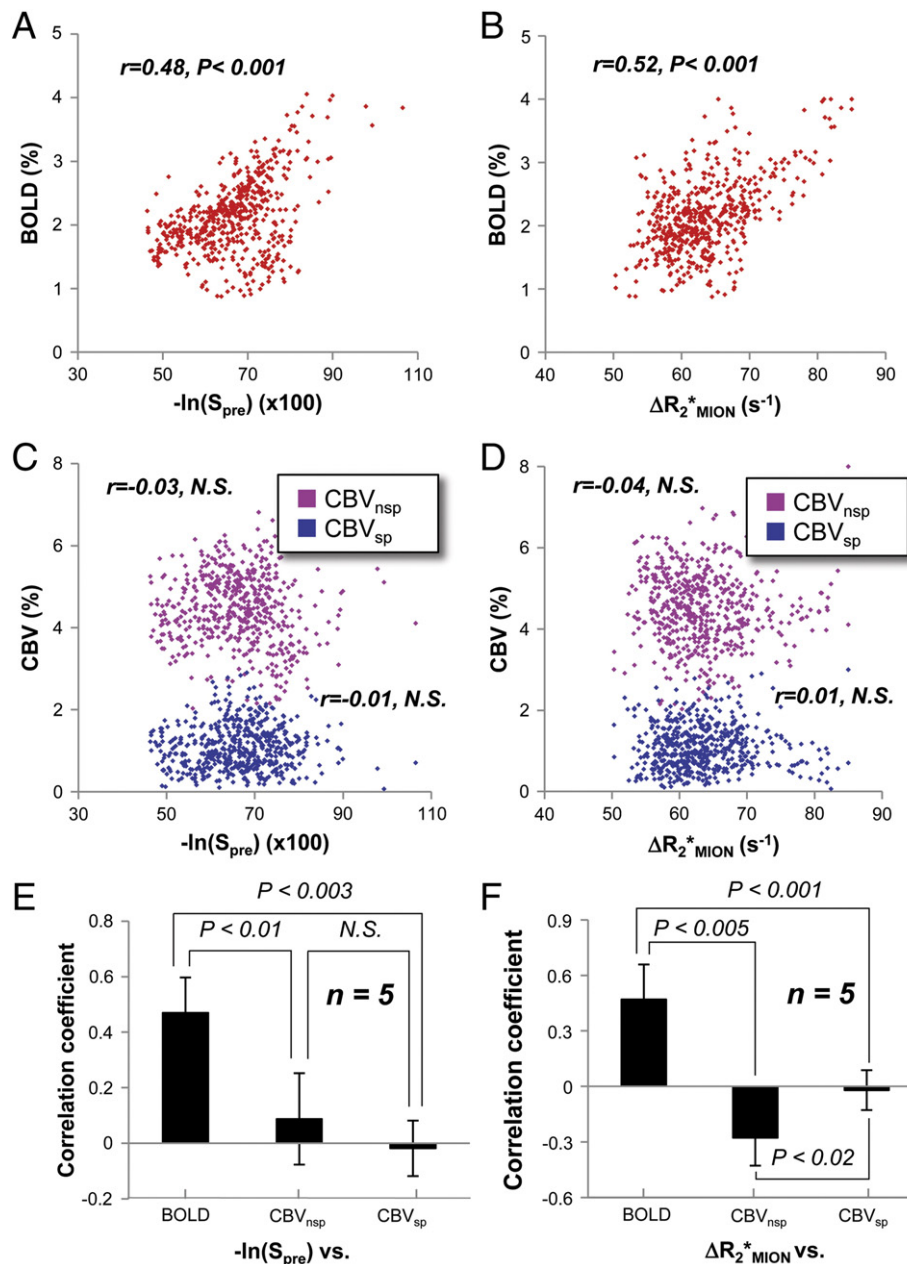


Fig. 6. Correlation between baseline blood volume maps and functional maps. A and B, Scatter plots of baseline venous CBV index, $-\ln(S_{pre})$ and total CBV, ΔR_{2MION}^* (Figs. 5C and D) vs. nonspecific BOLD map (Fig. 5E) in one animal. C and D, Scatter plots of baseline venous and total CBV vs. nonspecific and specific CBV maps (Figs. 5F and G) in one animal. E and F, Bar graphs of group-averaged correlation coefficients. Data are $Mean \pm SD$ of five cats. BOLD_{nsp(sp)} and CBV_{nsp(sp)} stand for the orientation-nonspecific (-specific) BOLD and CBV signals, respectively. Note that only the BOLD signal is significantly associated with the baseline venous and total CBV values.

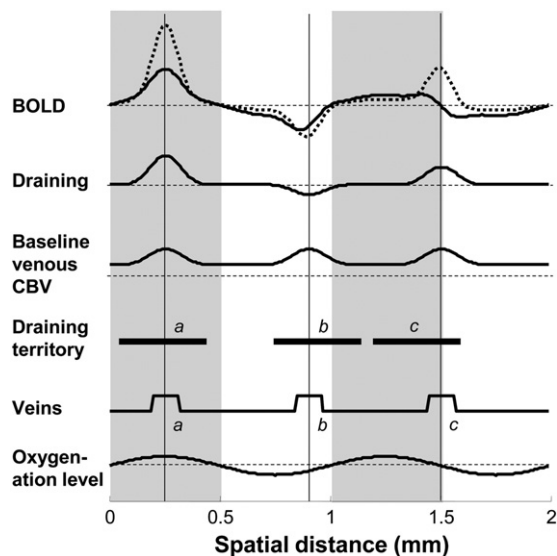


Fig. 7. Schematics of differential BOLD signals specific to columns. BOLD profiles with (black-dotted trace) and without (black trace) draining artifacts are compared. For the estimation of BOLD signals, multiple assumptions were made: 1) the venous CBV functional change is negligible, so the change in deoxyhemoglobin contents (relevant to BOLD) is the product of a change in total oxygenation level and baseline CBV. 2) Oxygenation-level change at capillaries obtained from the differential analysis is assumed to be localized to the neuronal sites with 500- μm full-width-half-maximum. 3) Intracortical veins are assumed to have 100- μm width, and contribute to the baseline CBV with a blurring effect (see baseline venous CBV). Three hypothetical veins' positions relative to columns are considered. Veins *a*, *b* and *c* are positioned in the center of an active column (gray regions), in an inactive column (white regions) shifted from its center, and in the boundary of active and inactive columns, respectively. Black vertical lines indicate the centers of the individual veins. Hypothetical draining territories of these individual veins (horizontal black bars marked with the same letters) and their draining effects are shown. The amount of draining in the vein was simulated by summation of oxygenation levels from given draining territories, then added to the oxygenation level change in capillaries to obtain the total oxygenation level change in each pixel. Black-dotted horizontal lines are the baselines of signal changes. Note that the BOLD localization to neuronal sites is even more distorted due to nonspecific draining artifacts to intracortical veins than only baseline venous CBV.

data were obtained within the iso-orientation ROIs (see **Methods and materials**). The averaged preferred and nonpreferred responses for 20-s and 10-s block-design studies were plotted, as well as normalized responses to compare the dynamic properties (Fig. 4). The magnitudes of preferred and nonpreferred BOLD responses were similar regardless of the orientation stimuli used (Figs. 4A and D), while the preferred CBV responses were higher than the nonpreferred responses (Figs. 4B and E). Thus, neural-specific signals were detectable only in the CBV data under the current block-design stimulation paradigms (black traces in Figs. 4B and E). In both fMRI modalities, orientation-nonspecific signals (red traces) were dominant compared to the orientation-specific signals (black traces). The average signal change at the steady state began 6 s after stimulus onset and continued to the end of stimulus. For 10-s stimulus data, nonspecific BOLD and CBV changes were respectively $1.63 \pm 0.34\%$ and $4.59 \pm 1.29\%$ ($n = 5$ cats), and the specific CBV change was $1.48 \pm 0.56\%$ ($n = 5$ cats). For 20-s stimulus data, nonspecific BOLD and CBV signals were respectively $1.95 \pm 0.93\%$ and $4.78 \pm 1.54\%$ ($n = 5$ cats), and the specific CBV signal was $1.87 \pm 1.17\%$ ($n = 5$ cats).

The time constants (i.e., response time at 70% of peak points) of functional responses were measured from the mean response of five cats for 20-s stimulation: ~ 4.9 s, ~ 4.3 s, and ~ 9.4 s for nonspecific BOLD and CBV, and specific CBV, respectively (Fig. 4C). These time constants suggest that the specific CBV response is delayed from the

nonspecific CBV response. Similar characteristics of functional responses exist in 10-s stimulus data (Fig. 4F).

The CBV spatial specificity index increased with the stimulation time. For 10-s stimulus data, the spatial specificity indices at 3–5 s, 9–12 s and 12–14 s were 0.18 ± 0.05 , 0.31 ± 0.05 , and 0.48 ± 0.12 ($n = 5$ cats), respectively. For 20-s stimulus data, the spatial specificity indices at 3–5 s, 9–12 s, 17–20 s, and 23–25 s were 0.17 ± 0.15 , 0.26 ± 0.12 , 0.33 ± 0.12 , and 0.43 ± 0.20 ($n = 5$ cats), respectively. Our results are similar to the values obtained at steady-state conditions under 20-s stimulation, 0.31 to 0.48 (Zhao et al., 2005).

Vascular sources of parenchymal BOLD and CBV signals

To examine the relationships between high-resolution fMRI activation maps and cortical vessels, intracortical emerging veins were identified by those hypo-intensities in T_2^* -weighted anatomical image (Figs. 5A and B); emerging veins appear as dark spots in the T_2^* -weighted images. The appearance of vessel diameter in T_2^* -weighted anatomical image is much larger than the actual vessel size due to the extended susceptibility effect induced by intravessel deoxyhemoglobin (Park et al., 2008). The sites of intracortical veins (blue crosses in Fig. 5B) were compared to baseline blood volume maps and fMRI activation foci. Cross-correlation coefficient between $-\ln(S_{pre})$ and ΔR_{2MION}^* (i.e., baseline blood volume before and after the MION injection) was 0.17 ± 0.29 ($P < 0.0001$, $n = 5$ cats). Higher local susceptibility effect reduces baseline signal intensity, thus higher $-\ln(S_{pre})$ value (Fig. 5C) likely has a larger venous baseline CBV fraction. Meanwhile, ΔR_{2MION}^* (Fig. 5D) is directly related to the total baseline CBV fraction. Since 60%–75% of total CBV originates from venous CBV (Lee et al., 2001), foci (local hot spots) in $-\ln(S_{pre})$ and ΔR_{2MION}^* map were mostly located at or near intracortical veins (blue crosses in Figs. 5C and D).

In order to determine the vascular sources of neural-nonspecific and -specific functional signals, orientation-nonspecific and -specific maps (Figs. 5E–H) were compared to the baseline blood volume maps. Intracortical veins (blue crosses) were located in activation foci (local hot spots) of the orientation-nonspecific BOLD map (Fig. 5E), but not in those of the orientation-nonspecific CBV map (Fig. 5F). In the orientation-specific CBV magnitude map (Fig. 5G), high signal changes (red pixels) indicate high orientation selectivity, while zero signal changes (dark blue color, see white-solid dots) mean no orientation selectivity, which is likely to be fractures or pinwheel centers (see white solid dots in Fig. 5H) with no orientation preference (Bonhoeffer and Grinvald, 1993). Our CBV data showed that the location of intracortical venous vessels (white and black crosses in Figs. 5G and H) did not seem to be related to the orientation-column specific features (e.g., iso-orientation domains or pinwheel centers).

To quantitatively evaluate the vascular sources of functional maps, pixel-wise relationships between the baseline blood volume maps and the activation maps (Fig. 5) are plotted in Fig. 6. In one subject's high-resolution data, the $-\ln(S_{pre})$ and ΔR_{2MION}^* values were linearly correlated with the BOLD signals (Figs. 6A and B), but not with either the orientation-nonspecific or -specific CBV signals (Figs. 6C and D). Similar results were obtained from the other four animals. The group-averaged correlation coefficient of all five animals was 0.47 ± 0.13 ($n = 5$ cats) for $-\ln(S_{pre})$ vs. orientation-nonspecific BOLD, 0.09 ± 0.17 for $-\ln(S_{pre})$ vs. orientation-nonspecific CBV, -0.02 ± 0.10 for $-\ln(S_{pre})$ vs. orientation-specific CBV; 0.47 ± 0.19 for ΔR_{2MION}^* vs. orientation-nonspecific BOLD, -0.28 ± 0.15 for ΔR_{2MION}^* vs. orientation-nonspecific CBV, and -0.02 ± 0.11 for ΔR_{2MION}^* vs. orientation-specific CBV (Figs. 6E and F). The orientation-nonspecific BOLD map was highly correlated with the baseline blood volume maps compared to the orientation-nonspecific or orientation-specific CBV maps ($P < 0.01$, $n = 5$ cats).

Discussion

The major findings of our submillimeter BOLD and CBV fMRI studies in the cat orientation column model are; 1) large CBV responses initially occur at pial arteries, while large BOLD responses are sustained at pial veins, 2) the orientation-nonspecific signal component is dominant in BOLD fMRI, and its foci are located at intracortical veins, and 3) the orientation-nonspecific CBV response is fast and reaches an early peak, while the orientation-specific CBV response is slower and sustained to the end of stimulation. These findings and their potential implications to neurovascular coupling will be discussed below. In order to examine the functional hemodynamic responses, it is important to review the pial and intracortical vasculatures. The pial arterial and venous vessels are numerous on the cortical surface, and are larger than the parenchymal vessels including intracortical vessels and capillaries (Duvernoy et al., 1981). The intracortical vasculature can be classified simply into macrovessels and microvessels; cortical macrovessels are penetrating arteries and emerging veins, while microvessels (<10 μm diameter) consist of arterioles (branched laterally off the penetrating arteries), pre-capillary arterioles, capillaries, post-capillary venules, and venules (branched laterally off the emerging veins). The diameter of intracortical arteries and veins has not been reported for cats to the best of our knowledge. Based on previous two-photon vascular imaging studies in rats, the diameter of penetrating vessels is 10–40 μm for arteries and 10–65 μm for veins (Park et al., 2008), and the density of penetrating vessels is ~ 60 arteries/ mm^2 (Nishimura et al., 2007) and ~ 14 veins/ mm^2 (see Fig. 5e in Park et al. (2008)). These intracortical vessels run perpendicular to the sagittal imaging plane, thus its intravoxel fraction in fMRI is relatively high. However, not all emerging veins are detectable by T_2^* -weighted anatomy MRI, and the density of MR-detectable veins with >16–30- μm diameter is ~ 3.8 veins/ mm^2 at the middle of the cortex in rats (see Fig. 4i in Park et al. (2008)).

Effect of anesthetics to hemodynamic responses

Before we discuss the implications of our findings to high-resolution fMRI studies, it is important to address the effect of isoflurane to evoked hemodynamic responses. Previous studies comparing functional hemodynamic responses in awake vs. isoflurane-anesthetized animals have been performed with visual stimulation in cats (Fukuda et al., 2005). Even though the magnitudes of responses are reduced with isoflurane by ~ 3 times (Fukuda et al., 2005; Zhao et al., 2007), columnar maps obtained from hemodynamic-based optical imaging are almost identical for awake and anesthetized conditions (Fukuda et al., 2005). Importantly, the general shape of deoxyhemoglobin (dHb)-weighted (analogous to BOLD) and total hemoglobin (i.e., CBV) response time-courses is similar for awake and anesthetized conditions. During 2-s stimulation, the time to the CBV peak is 4.2 s and 4.1 s in anesthetized and awake states respectively (Fukuda et al., 2005); the dHb response peak time is 5–6 s for both conditions (Zhao et al., 2007). Similar observations were seen in monkeys (Shtoyerman et al., 2000). Overall, the evoked hemodynamic dynamics and spatial patterns in isoflurane-anesthetized animals are similar to those in awake animals, albeit with reduced magnitude (Fukuda et al., 2005; Shtoyerman et al., 2000). Thus, we believe that our findings in the isoflurane-anesthetized condition are also applicable to the awake condition.

Intracortical vascular structure vs. BOLD fMRI: implication to high-resolution BOLD fMRI

The high-resolution BOLD fMRI signal is highly correlated to baseline venous CBV (Ogawa et al., 1993), and baseline total CBV. This finding is reasonable because the BOLD signal is directly related

to a change in deoxyhemoglobin contents, which is a combination of venous CBV and blood oxygenation level (Kim et al., 1999). Even if the venous blood oxygenation level change is similar across pixels, the BOLD signal is modulated by the baseline venous CBV fraction. A similar observation with high-resolution BOLD fMRI was reported in a study with rat somatosensory cortex (Yu et al., 2012), in which higher BOLD signal changes are located at the intracortical venous vessels.

The major implication of our high-resolution BOLD studies is the intrinsic limit of spatial resolution for mapping submillimeter functional units, such as orientation columns. Since the BOLD signal is sensitive to the intracortical veins emerging to the cortical surface, the inter-distance of the intracortical veins will be an important index for determining the spatial resolution of BOLD fMRI. The measured distance of nearest neighboring MR-detectable intracortical veins was ~ 500 μm in cat visual cortex (see Fig. 5B), and 300–500 μm in rats somatosensory area (Park et al., 2008). Thus, when the pixel resolution of fMRI (e.g., <160 μm) is higher than the inter-distance between nearest neighboring intracortical veins of ~ 500 μm apart, then we believe that the pixel-wise BOLD signal will be heavily weighted by uneven venous blood volume, even if neural activity, cerebral blood flow (CBF), and venous oxygenation changes are identical. In addition, each vein has upstream vascular territory, which is unknown (Duvernoy et al., 1981). When a functional structure is smaller than the inter-vein distance or fMRI resolution is higher than the inter-vein distance, then the activation sites determined by BOLD fMRI may be shifted or distorted from the genuine functional domain (see Fig. 7).

In submillimeter resolution fMRI studies, nonspecific BOLD signals at emerging veins are dominant. In order to detect small neural-specific functional signals, the effects of nonspecific components on specific components must be minimized. Three approaches can be considered; 1) differential data analysis, 2) appropriate paradigm design, and 3) better data collection technique sensitive to small vessels. When the domains responding to orthogonal stimuli are complementary, such as ocular dominance and orientation columns, the differential method works well (see Fig. 7). However, the differential method is not sufficient in our BOLD studies, since the physiological fluctuation in the nonspecific component is probably higher than small orientation-specific signals of $\sim 0.3\%$ (Moon et al., 2007). Alternatively, more advanced statistical methods such as principal component analysis may be applied to separate nonspecific macrovascular signals from microvascular signals before the application of the differential approach (Vanzetta et al., 2004a). To reduce the macrovascular contribution and nonspecific signals, continuous cyclic stimulation can be adapted (Moon et al., 2007). With continuous stimulation, the orientation-nonspecific signal decreases, while only the orientation-specific signal is modulated by the cyclical stimulation; Fourier analysis can then be effectively applied to extract the periodic orientation-selective component from the time-series data. Further, macrovascular contributions to the BOLD fMRI signal can be removed by spin-echo (SE) approach. SE BOLD reduces venous draining artifacts, and increases the functional specificity to active columns, but with reduced sensitivity compared to GE BOLD (Moon et al., 2007). Thus, if SE BOLD fMRI has sufficient sensitivity, then it will be a good alternative approach at high fields (Yacoub et al., 2008).

Failure to detect orientation-specific BOLD signals

In our present BOLD data using block-design stimulation, we did not find an orientation-specific signal, which is similar to our previous findings (Kim et al., 2000; Moon et al., 2007) that nonspecific BOLD signals are dominant for both 10-s and 20-s block-design orientation stimulation. In our previous BOLD column studies (Moon et al., 2007) with 312- μm in-plane resolution and continuous cyclic

stimulation, the iso-orientation columns obtained from BOLD fMRI corresponded well with those by optical imaging. The differences between our current and previous BOLD fMRI studies are higher spatial resolution (i.e., 156 vs. 312 μm) and stimulation paradigm (i.e., block-design vs. continuous cyclic stimulation), both of which can impact columnar-resolution functional mapping capability. As mentioned above, higher spatial resolution fMRI induces less homogeneous vascular contribution to the BOLD signal, resulting in larger vascular problems in our current high-resolution BOLD data.

To reduce large vessel problems, the early positive BOLD or early negative dip may be used before specific capillary blood drain into less specific, large venous vessels. The early positive BOLD response may potentially be able to resolve orientation columns due to the improved spatial specificity (Goodyear and Menon, 2001; Shmuel et al., 2007; Yu et al., 2012). Alternatively, even if it is difficult to be reliably detected, the early BOLD dip can be used (Kim et al., 2000; Malonek and Grinvald, 1996). This early dip, albeit its source is still controversial, has been commonly used in optical imaging for mapping columnar structures (Malonek and Grinvald, 1996; Shtoyerman et al., 2000). To capture the early dip or early positive BOLD responses, high spatial and temporal resolution fMRI are required as well as high sensitivity, which is technically challenging.

Dual spatiotemporal characteristics of CBV response: insight into CBV regulation

An interesting observation is to have high CBV-weighted fMRI signal changes at pial arteries (Fig. 1). This finding is consistent with previous studies of arterial and venous CBV (Drew et al., 2011; Kim and Kim, 2011); generally, the arterial vessels dilate quickly after stimulus onset, while the diameters of venous vessels increase slowly. Thus, 10-s and 20-s stimulation are not likely to induce the dilation in venous vessels significantly.

Parenchymal orientation-nonspecific and -specific CBV responses have different dynamic properties. The orientation-nonspecific CBV response component peaks faster than the orientation-specific CBV component, indicating that the CBV response localized to cortical columns is delayed. These findings appear to be inconsistent with CBV-based optical intrinsic signal data during 2-s forepaw stimulation (Sheth et al., 2005). This discrepancy is likely to be due to the relatively large contribution of the pial vessels to the optical signals; in our current study, the pial vessels were not included in functional imaging slice.

The orientation-nonspecific CBV response was negatively correlated with the baseline total CBV value, indicating that smaller vessels have larger percent changes (Drew et al., 2011; Lee et al., 2001), but the orientation-specific CBV signal was not correlated with baseline total CBV value (Fig. 6F). Orientation-nonspecific CBV component can be attributed to 1) the contribution of macrovessels which supply to or drain from multiple columns, and/or 2) the contribution of orientation-nonspecific microvessels. The fast nonspecific response is likely due to the major contribution of actively controlling arterial vessels, because venous vessels respond passively following the arterial response. A similar conclusion can be drawn by careful inspection of time-dependent CBV responses (Figs. 2 and 3), in which the pixels with large CBV changes at early time (see at 1–3 s) are not specific to orientation stimuli, indicating that the penetrating arteries (less than 50- μm diameter) are not co-localized with columnar domains (see black arrowheads in Fig. 5D); thus those dilations are not sufficient for column-specific blood flow supplies. No correlation between penetrating arterial domains and underlying barrels was also reported in the whisker barrel field (Woolsey et al., 1996). Meanwhile, the orientation-specific component must then originate from microvessels, possibly including small pre-capillary arterioles and capillaries with the requirement of an active control mechanism.

Spatiotemporal properties of our CBV responses are consistent with previous layer-dependent CBV studies (Jin and Kim, 2008; Kim and Kim, 2010, 2011). In layer-dependent studies, the early CBV response (at 3–5 s following stimulus onset) mostly occurs at upper cortical layers and along the radial direction of cortex, while a slow and delayed response (> 10 s) is much better localized to the middle of the cortex where microvessels are dominant. These MR data are consistent with spectroscopic optical imaging studies of rat somatosensory with 16-s whisker stimulation (Berwick et al., 2008), in which a transient response in the upstream branches of pial arteries is followed by a later highly localized increase in CBV centered on the activated cortical whisker barrel, indicating that the late response occurs at cortical microvessels. Capillary CBV increases have also been suggested by other CBV-based optical imaging studies (Frostig et al., 1990; Fukuda et al., 2005; Narayan et al., 1995; Vanzetta et al., 2004b) according to their ability to map cortical columns with CBV. Similarly, microvascular blood volume increase (< 10- μm diameter) was observed with multiphoton microscopy during 60-s forepaw stimulation in rats (Stefanovic et al., 2007). These capillary dilations contribute to column-specific CBV signals.

To precisely control functional CBF and CBV responses in a localized area, both active and passive control mechanisms co-exist and possibly interact. Active control occurs at a coarse scale in upstream arterial vessels and at a fine scale, possibly at capillaries, while passive control mechanism can be explained by the Windkessel compliance model (Mandeville et al., 1999). Increased neural activity results in vasoactive signals being sent into nearby capillaries and arterioles via astrocyte endfeet or via other mediators (Attwell et al., 2010). Then, information spreads retrogradely to upstream arterial parenchymal and pial vessels (Iadecola et al., 1997; Tian et al., 2010), inducing arterial vessel dilations. Simultaneously, the pericytes and/or sphincters at strategically important points of pre-capillary arterioles and capillaries, feeding to the active region, may respond to increased blood flow at the active domain (Bell et al., 2010). When arterial vessels dilate, the upstream segmental blood pressure difference (ΔP_{a-c}) between arteries and microvessels decreases, while downstream segmental blood pressure difference (ΔP_{c-v}) between microvessels and veins increases, assuming the arterial-venous blood pressure difference ($\Delta P_{a-v} = \Delta P_{a-c} + \Delta P_{c-v}$) is constant. The increase in the downstream ΔP_{c-v} (and CBF) will slowly induce dilations of small arterioles, possibly capillaries, and finally venous vessels. Dilation in downstream vessels decreases downstream resistance (R), which will consequently reduce downstream ΔP_{c-v} . This downstream ΔP_{c-v} adjustment may send retrograde signals to increase initially-decreased upstream ΔP_{a-c} and R for maintaining constant CBF change and ΔP_{a-v} . Then, the magnitude of dilation in upstream vessels is reduced to a steady state. These active and passive CBV control mechanisms dynamically modulate dilations of different vessel segments. Following stimulus offset, the orientation-nonspecific macrovessels component decays faster than the orientation-specific microvessel component, similar to the responses to the stimulus onset (see Fig. 4). The CBV localization is improved when the dilation of upstream macrovessels is reduced after the initial adjustment during the stimulation period or after stimulus offset, but before downstream macrovessels dilations are significant.

Conclusions

Highest gradient-echo BOLD signal changes were observed in pial veins and parenchymal intracortical veins. The positive BOLD response was dominantly neural-nonspecific even at ultrahigh submillimeter resolution, and was highly correlated with baseline blood volume. Consequently, neural-specific functional domains could be displaced or distorted in high-resolution BOLD maps if imaging voxel resolution is higher than the distance between neighboring

inter-emerging veins. In contrary, the CBV response had early neural-nonspecific and delayed neural-specific components. The nonspecific CBV signal originates from early-responding upstream arteries and arterioles, while the specific CBV response arises from late-responding microvessels including small pre-capillary arterioles and capillaries. Therefore, high-resolution functional maps can be obtained from steady state CBV studies.

Acknowledgments

We thank Ping Wang for animal preparation and David Whitney for reviewing and editing the manuscript. This work was supported by NIH (NS44589, EB003324, and EB003375), and was presented in part at the 17th Annual Meeting of the International Society for Magnetic Resonance in Medicine.

Appendix A. Supplementary data

Supplementary data to this article can be found online at <http://dx.doi.org/10.1016/j.neuroimage.2012.08.064>.

References

- Attwell, D., Buchan, A.M., Chrapak, S., Lauritzen, M., MacVicar, B.A., Newman, E.A., 2010. Glial and neuronal control of brain blood flow. *Nature* 468, 232–243.
- Bell, R.D., Winkler, E.A., Sagare, A.P., Singh, I., LaRue, B., Deane, R., Zlokovic, B.V., 2010. Pericytes control key neurovascular functions and neuronal phenotype in the adult brain and during brain aging. *Neuron* 68, 409–427.
- Berwick, J., Johnston, D., Jones, M., Martindale, J., Martin, C., Kennerley, A.J., Redgrave, P., Mayhew, J.E.W., 2008. Fine detail of neurovascular coupling revealed by spatio-temporal analysis of the hemodynamic response to single whisker stimulation in rat barrel cortex. *J. Neurophysiol.* 99, 787–798.
- Bonhoeffer, T., Grinvald, A., 1993. The layout of iso-orientation domains in area 18 of cat visual cortex: optical imaging reveals a pin-wheel-like organization. *J. Neurosci.* 13, 4157–4180.
- Chen, L.M., Turner, G.H., Friedman, R.M., Zhang, N., Gore, J.C., Roe, A.W., Avison, M.J., 2007. High-resolution maps of real and illusory tactile activation in primary somatosensory cortex in individual monkeys with functional magnetic resonance imaging and optical imaging. *J. Neurosci.* 27, 9181–9191.
- Cheng, K., Waggoner, R., Tanaka, K., 2001. Human ocular dominance columns as revealed by high-field functional magnetic resonance imaging. *Neuron* 32, 359–374.
- Cox, S.B., Woolsey, T.A., Rovainen, C.M., 1993. Localized dynamic changes in cerebral blood flow in rat barrel cortex with whisker stimulation. *J. Cereb. Blood Flow Metab.* 13, 899–913.
- Das, A., Gilbert, C.D., 1995. Long-range horizontal connections and their role in cortical reorganization revealed by optical recording of cat primary visual cortex. *Nature* 375, 780–784.
- Dechent, P., Frahm, J., 2000. Direct mapping of ocular dominance columns in human primary visual cortex. *Neuroreport* 11, 3247–3249.
- Drew, P.J., Shih, A.Y., Kleinfeld, D., 2011. Fluctuating and sensory-induced vasodynamics in rodent cortex extend arteriole capacity. *Proc. Natl. Acad. Sci.* 108, 8473–8478.
- Duong, T.Q., Kim, D.-S., Ugurbil, K., Kim, S.-G., 2001. Localized cerebral blood flow response at submillimeter columnar resolution. *Proc. Natl. Acad. Sci.* 98, 10904–10909.
- Duvernoy, H., Delon, S., Vannson, J., 1981. Cortical blood vessels of the human brain. *Brain Res.* Brain 7, 519–579.
- Frostig, R.D., Lieke, E.E., Ts'o, D.Y., Grinvald, A., 1990. Cortical functional architecture and local coupling between neuronal activity and the microcirculation revealed by in vivo high-resolution optical imaging of intrinsic signals. *Proc. Natl. Acad. Sci.* 87, 6082–6086.
- Fukuda, M., Rajagopalan, U.M., Homma, R., Matsumoto, M., Nishizaki, M., Tanifuji, M., 2005. Localization of activity-dependent changes in blood volume to submillimeter-scale functional domains in cat visual cortex. *Cereb. Cortex* 15, 823–833.
- Fukuda, M., Moon, C.-H., Wang, P., Kim, S.-G., 2006a. Mapping iso-orientation columns by contrast agent-enhanced functional magnetic resonance imaging: reproducibility, specificity, and evaluation by optical imaging of intrinsic signal. *J. Neurosci.* 26, 11821–11832.
- Fukuda, M., Wang, P., Moon, C.H., Tanifuji, M., Kim, S.G., 2006b. Spatial specificity of the enhanced dip inherently induced by prolonged oxygen consumption in cat visual cortex: implication for columnar resolution functional MRI. *Neuroimage* 30, 70–87.
- Goodyear, B., Menon, R.S., 2001. Brief visual stimulation allows mapping of ocular dominance in visual cortex using fMRI. *Hum. Brain Mapp.* 14, 210–217.
- Grinvald, A., Leike, E., Frostig, R.D., Gillbert, C.D., Wiesel, T.N., 1986. Functional architecture of cortex revealed by optical imaging of intrinsic signals. *Nature* 324, 361–364.
- Hubel, D., Wiesel, T., 1962. Receptive fields, binocular interactions and functional architecture in the cat's visual cortex. *J. Physiol. Lond.* 160, 106–154.
- Hubel, D.H., Wiesel, T.N., 1963. Shape and arrangement of columns in cat's striate cortex. *J. Physiol.* 165, 559–568.
- Iadecola, C., Yang, G., Ebner, T.J., Chen, G., 1997. Local and propagated vascular responses evoked by focal synaptic activity in cerebellar cortex. *J. Neurophysiol.* 78, 651–659.
- Jin, T., Kim, S.-G., 2008. Cortical layer-dependent dynamic blood oxygenation, cerebral blood flow and cerebral blood volume responses during visual stimulation. *Neuroimage* 43, 1–9.
- Kalatsky, V., Stryker, M.P., 2003. New paradigm for optical imaging: temporally encoded maps of intrinsic signal. *Neuron* 38, 529–545.
- Kim, T., Kim, S.-G., 2010. Cortical layer-dependent arterial blood volume changes: improved spatial specificity relative to BOLD fMRI. *Neuroimage* 49, 1340–1349.
- Kim, T., Kim, S.-G., 2011. Temporal dynamics and spatial specificity of arterial and venous blood volume changes during visual stimulation: implication for BOLD quantification. *J. Cereb. Blood Flow Metab.* 31, 1211–1222.
- Kim, S.-G., Hu, X., Adriany, G., Ugurbil, K., 1996. Fast interleaved echo-planar imaging with navigator: high resolution anatomic and functional images at 4 Tesla. *Magn. Reson. Med.* 35, 895–902.
- Kim, S.-G., Rostrup, E., Larsson, H.B.W., Ogawa, S., Paulson, O.B., 1999. Determination of relative CMRO₂ from CBF and BOLD changes: significant increase of oxygen consumption rate during visual stimulation. *Magn. Reson. Med.* 41, 1152–1161.
- Kim, D.-S., Duong, T.Q., Kim, S.-G., 2000. High-resolution mapping of iso-orientation columns by fMRI. *Nat. Neurosci.* 3, 164–169.
- Lee, S.-P., Duong, T., Yang, G., Iadecola, C., Kim, S.-G., 2001. Relative changes of cerebral arterial and venous blood volumes during increased cerebral blood flow: implications for BOLD fMRI. *Magn. Reson. Med.* 45, 791–800.
- Löwel, S., Freeman, B., Singer, W., 1987. Topographic organization of the orientation column system in large flat-mounts of the cat visual cortex: a 2-deoxyglucose study. *J. Comp. Neurol.* 255, 401–415.
- Malonek, D., Grinvald, A., 1996. Interactions between electrical activity and cortical microcirculation revealed by imaging spectroscopy: implication for functional brain mapping. *Science* 272, 551–554.
- Mandeville, J.B., Marota, J.J.A., Kosofsky, B.E., Keltner, J.R., Weissleder, R., Rosen, B.R., 1998. Dynamic functional imaging of relative cerebral blood volume during rat forepaw stimulation. *Magn. Reson. Med.* 39, 615–624.
- Mandeville, J.B., Marota, J.J.A., Ayata, C., Zaharchuk, G., Moskowitz, M.A., Rosen, B.R., Weisskoff, R.M., 1999. Evidence of a cerebrovascular postarteriole Windkessel with delayed compliance. *J. Cereb. Blood Flow Metab.* 19, 679–689.
- Menon, R.S., Ogawa, S., Strupp, J.P., Ugurbil, K., 1997. Ocular dominance in human V1 demonstrated by functional magnetic resonance imaging. *J. Neurophysiol.* 77, 2780–2787.
- Moon, C.-H., Fukuda, M., Park, S.-H., Kim, S.-G., 2007. Neuronal interpretation of blood oxygenation level-dependent fMRI maps at submillimeter columnar resolution. *J. Neurosci.* 27, 6892–6902.
- Mountcastle, V.B., 1957. Modality and topographic properties of single neurons of cat's somatic sensory cortex. *J. Neurophysiol.* 20, 408–434.
- Nagaoka, T., Zhao, F., Wang, P., Harel, N., Kennan, R.P., Ogawa, S., Kim, S.-G., 2005. Increases in oxygen consumption without cerebral blood volume change during visual stimulation under hypotension condition. *J. Cereb. Blood Flow Metab.* 26, 1043–1051.
- Narayan, S.M., Esfahani, P., Blood, A.J., Sikkens, L., Toga, A.W., 1995. Functional increases in cerebral blood volume over somatosensory cortex. *J. Cereb. Blood Flow Metab.* 15, 754–765.
- Nishimura, N., Schaffer, C.B., Friedman, B., Lyden, P.D., Kleinfeld, D., 2007. Penetrating arterioles are a bottleneck in the perfusion of neocortex. *Proc. Natl. Acad. Sci.* 104, 365–370.
- Ogawa, S., Lee, T.M., Barrere, B., 1993. Sensitivity of magnetic resonance image signals of a rat brain to changes in the cerebral venous blood oxygenation. *Magn. Reson. Med.* 29, 205–210.
- Park, S.-H., Masamoto, K., Hendrich, K., Kanno, I., Kim, S.-G., 2008. Imaging brain vasculature with BOLD microscopy: MR detection limits determined by in vivo two-photon microscopy. *Magn. Reson. Med.* 59, 855–865.
- Sheth, S.A., Nemoto, M., Guio, M.W., Walker, M.A., Toga, A.W., 2005. Spatiotemporal evolution of functional hemodynamic changes and their relationship to neuronal activity. *J. Cereb. Blood Flow Metab.* 25, 830–841.
- Shmuel, A., Yacoub, E., Chaimow, D., Logothetis, N.K., Ugurbil, K., 2007. Spatio-temporal point-spread function of fMRI signal in human gray matter at 7 Tesla. *Neuroimage* 35, 539–552.
- Shmuel, A., Chaimow, D., Raddatz, G., Ugurbil, K., Yacoub, E., 2010. Mechanisms underlying decoding at 7 T: ocular dominance columns, broad structures, and macroscopic blood vessels in V1 convey information on the stimulated eye. *Neuroimage* 49, 1957–1964.
- Shoham, D., Glaser, D.E., Arieli, A., Kenet, T., Wijnbergen, C., Toledo, Y., Hildesheim, R., Grinvald, A., 1999. Imaging cortical dynamics at high spatial and temporal resolution with novel blue voltage-sensitive dyes. *Neuron* 24, 791–802.
- Shtoyerman, E., Arieli, A., Slovlin, H., Vanzetta, I., Grinvald, A., 2000. Long-term optical imaging and spectroscopy reveal mechanisms underlying the intrinsic signal and stability of cortical maps in V1 of behaving monkeys. *J. Neurosci.* 20, 8111–8121.
- Stefanovic, B., Hutchinson, E., Yakovleva, V., Schram, V., Russell, J.T., Belluscio, L., Koretsky, A.P., Silva, A.C., 2007. Functional reactivity of cerebral capillaries. *J. Cereb. Blood Flow Metab.* 28, 961–972.
- Tanaka, S., Moon, C.-H., Fukuda, M., Kim, S.-G., 2011. Three-dimensional visual feature representation in the primary visual cortex. *Neural Netw.* 24, 1022–1035.
- Tian, P., Teng, I.C., May, L.D., Kurz, R., Lu, K., Scadeng, M., Hillman, E.M.C., De Crespigny, A.J., D'Arceuil, H.E., Mandeville, J.B., Marota, J.J.A., Rosen, B.R., Liu, T.T., Boas, D.A., Buxton, R.B., Dale, A.M., Devor, A., 2010. Cortical depth-specific microvascular dilation underlies laminar differences in blood oxygenation level-dependent functional MRI signal. *Proc. Natl. Acad. Sci.* 107, 15246–15251.
- Vanzetta, I., Slovlin, H., Omer, D., Grinvald, A., 2004a. Columnar resolution of blood volume and oximetry functional maps in the behaving monkey; implications for fMRI. *Neuron* 42, 843–854.

- Vanzetta, I., Slovin, H., Omer, D.B., Grinvald, A., 2004b. Columnar resolution of blood volume and oximetry functional maps in the behaving monkey. *Neuron* 42, 843–854.
- Woolsey, T.A., Van der Loos, H., 1970. The structural organization of layer IV in the somatosensory region (SI) of mouse cerebral cortex: the description of a cortical field composed of discrete cytoarchitectonic units. *Brain Res.* 17, 205–242.
- Woolsey, T.A., Rovainen, C.M., Cox, S.B., Henegar, M.H., Liang, G.E., Liu, D., Moskalenko, Y.E., Sui, J., Wei, L., 1996. Neuronal units linked to microvascular modules in cerebral cortex: response elements for imaging the brain. *Cereb. Cortex* 6, 647–660.
- Yacoub, E., Harel, N., Ugurbil, K., 2008. High-field fMRI unveils orientation columns in humans. *Proc. Natl. Acad. Sci.* 105, 10607–10612.
- Yu, X., Glen, D., Wang, S., Dodd, S., Hirano, Y., Saad, Z., Reynolds, R., Silva, A.C., Koretsky, A.P., 2012. Direct imaging of macrovascular and microvascular contributions to BOLD fMRI in layers IV–V of the rat whisker-barrel cortex. *Neuroimage* 9, 1451–1460.
- Zhao, F., Wang, P., Hendrich, K., Kim, S.-G., 2005. Spatial specificity of cerebral blood volume-weighted fMRI responses at columnar resolution. *Neuroimage* 27, 416–424.
- Zhao, F., Wang, P., Hendrich, K., Ugurbil, K., Kim, S.-G., 2006. Cortical layer-dependent BOLD and CBV responses measured by spin-echo and gradient-echo fMRI: insights into hemodynamic regulation. *Neuroimage* 30, 1149–1160.
- Zhao, F., Jin, T., Wang, P., Kim, S.-G., 2007. Isoflurane anesthesia effect in functional imaging studies. *Neuroimage* 38, 3–4.